Struct Multidisc Optim (2015) 52:71–90
DOI 10.1007/s00158-015-1286-0

RESEARCH PAPER

Structural topology optimization for maximum linear buckling loads by using a moving iso-surface threshold method

Quantian Luo · Liyong Tong

Received: 23 November 2013 / Revised: 16 November 2014 / Accepted: 26 November 2014 / Published online: 19 June 2015

Abstract This paper investigates topology design optimization for maximizing critical buckling loads of thin-walled structures using a moving iso-surface threshold (MIST) method. Formulation for maximizing linear buckling loads with additional constraints on load-path continuity and lower bound of eigenvalue is firstly presented. New physical response functions are proposed and expressed in terms of the strain energy densities determined in the two-steps of finite element buckling analysis. A novel approach by introducing a connectivity coefficient is developed to ensure continuity of effective load-path in optimum topology. The lower bound of eigenvalue is defined to eliminate spurious localized buckling modes. The MIST algorithm and its interfaces with commercial finite element (FE) software are given in detail. Numerical results are presented for topology optimization of plate-like structures to maximize critical buckling forces or displacements considering in-plane and out-of-plane buckling respectively. The FE analyses of the re-meshed final solid topologies with and without void material reveal that the presence of the void material has a significant effect on the out-of-plane buckling loads and a minor influence on the in-plane buckling loads.

Keywords Topology optimization · Buckling · Eigenvalue · Physical response function

Nomenclature

[**B**]	Strain–displacement matrix
[**D**]	Elastic constant matrix
[**K**]	Structural stiffness matrix
[$\mathbf{K}_\sigma$]	Structural geometric stiffness matrix
[**k**]	Elemental stiffness matrix
[$\mathbf{k}_\sigma$]	Elemental geometric stiffness matrix
[**N**]	Shape function matrix
[**u**]	Vector of physical displacements
[**F**]	Vector denoting external loadings
{**Y**}	Eigenvector
Φ	Physical response function
Ω	Design domain
λ_1	The 1st order eigenvalue
$\lambda_{\min}$	The lower bound of eigenvalue
k_1	Generalized stiffness for the 1st order mode
$k_{\sigma 1}$	Generalized geometric stiffness for mode 1
E_s	Total strain energy in static analysis
E_{sd}	Strain energy density in static analysis
E_λ	Total strain energy for the 1st order buckling mode
$E_{\lambda d}$	Strain energy density for buckling mode 1
N_e	Total element number
N_n	Total node number
t	The level or threshold value of the iso-surface S
V_e	Element volume with solid materials
V_0	Structure volume with solid materials
V_f	Volume fraction
x_e	Weighting factor ranging from 0 to 1
E	Young's modulus
ν	Poisson's ratio
e	Subscript for the eth element

Q. Luo · L. Tong (✉)
School of Aerospace, Mechanical and Mechatronic Engineering, The University of Sydney, Sydney, NSW 2006, Australia
e-mail: liyong.tong@sydney.edu.au

1 Introduction

Topology optimization has drawn much attention since 1980s due to its importance and enormous potential applications in practical structural design to meet specific structural performance requirements (Bendsoe and Sigmund 2003; Rozvany 2009). Optimization for a structure to achieve maximum

buckling load using a given amount of material represents one of these important applications (Neves et al. 1995; Manickarajah et al. 1998; Lund 2009; Lindgaard and Dahl 2013). A number of optimization methods have been used for structural topology design considering buckling, e.g., a solid isotropic material with penalisation (SIMP) method, (Bendsøe and Triantafyllidis 1990; Neves et al. 1995; Sekimoto and Noguchi 2001; Lindgaard and Dahl 2013), evolutionary structural optimization (ESO) (Manickarajah et al. 1998, 2000; Rong et al. 2001) and a level set method (LSM) (Kasaiezadeh et al. 2010; Zhao et al. 2011). In this paper, a moving iso-surface threshold method (MIST) recently developed (Tong and Lin 2011; Vasista and Tong 2012) will be used to address the following challenging issues in linear buckling optimization.

Topology optimization considering structural buckling is quite complicated and convergence is often relatively poor (Neves et al. 2002; Bendsoe and Sigmund 2003; Rahmatalla and Swan 2003; Bruyneel et al. 2008) owing to a number of issues, e.g.: (a) omitting stress state variations in sensitivity analysis, (b) spurious local buckling, (c) multiple mode shapes, and (d) lack of effective load-path. Issues (a) and (b) are mainly caused by the properties of a geometric stiffness matrix (GSM) in buckling analysis and problems (c) and (d) are typically observed in topology optimization involving solving eigenvalue problems. In addition, the widely used method of moving asymptotes (MMA) may encounter numerical difficulties as it uses the current iterative values of an objective function and its derivative (Browne et al. 2012); the buckling load may be artificially overestimated owing to the effects of low density materials (Zhou 2004).

In an iterative process of optimization, the buckling analysis comprises of solving a static stress analysis and a generalized eigenvalue problem. Geometric stiffness matrix (GSM) in the buckling analysis is a function of both design variables and global displacements/stresses determined from the static stress analysis. The global displacements or stresses are functions of design variables, however, in the sensitivity analysis of the GSM, their influences are often neglected, e.g., by ignoring the terms containing their derivatives with respect to the design variables, for the purpose of simplification in coding and of reducing computational costs (Neves et al. 1995; Mateus et al. 1997; Bruyneel et al. 2008). In doing so, the sensitivity analysis of buckling optimization is treated in the same way as that of a free vibration problem, which has been considered one of the error sources in a gradient-based optimization method for buckling analysis (Neves et al. 1995; Mateus et al. 1997; Bruyneel et al. 2008). As explicit sensitivity analysis is not conducted in MIST (Tong and Lin 2011; Vasista and Tong 2012), issue (a) is not involved in the iterative processes.

The GSM may be positive definite or indefinite during iterations. The indefinite GSM can result in negative eigenvalue λ_1 (Bendsoe and Sigmund 2003). In the optimization to maximize buckling load, it is required that $\lambda_1>0$. When design variables representing material densities in a region are too small, the mode shape corresponding to the 1st order eigenvalue (λ_1) may be localized in the region where the elements have low density (Tenek and Hagiwara 1994; Ben-Tal et al. 2000; Neves et al. 2002; Pedersen and Nielsen 2003). This spurious localized mode can be eradicated by re-meshing to remove the void elements with low density or by changing the stiffness and/or stresses of the void elements (Tenek and Hagiwara 1994; Ben-Tal et al. 2000; Neves et al. 2002; Pedersen and Nielsen 2003), e.g., by reducing stress in the elements with density lower than 10 % to an insignificant value (e.g., 10^{-15}) (Neves et al. 1995; Ben-Tal et al. 2000; Pedersen 2000; Bruyneel et al. 2008). In the present algorithm, the constraint of $\lambda_1>\lambda_{min}>0$ is introduced to enable the use of only the mode shape corresponding to this constraint in the construction of the response function and thus to allow elimination of the spurious localized mode.

In an iterative process for eigenvalue analysis, repetitive eigenvalues may appear. When eigenvalue λ_1 is repeated, the correct eigenvector may not be selected owing to multiple eigenvectors, which leads to mode switching and subsequently slows down convergence or even causes iterative divergence. A linear combination of eigenvalues or average-mean eigenvalues can be used as an objective function to prevent the mode switch in optimization to maximize a specific eigenvalue (Ma et al. 1995; Neves et al. 2002; Du and Olhoff 2007; Niu et al. 2009). A mode tracking technique can also be used (Eldred et al. 1995; Bruyneel et al. 2008) to monitor the mode switch and it will be used in the present MIST computing.

In the MIST iteration, a moving iso-surface threshold level is sought for the chosen response function and the prescribed constraints to update weighting factors; MMA is not used in the present algorithm.

A solution of topology optimization for eigenvalue problems can be trivial (e.g., optimization to maximize eigenvalue λ_1 of a cantilever plate vibration can be achieved by directly removing materials from the free edge.) or an obtained optimal design lacks an effective load-path, particularly for plate structures (Bendsoe and Sigmund 2003). In this case, artificial reinforcements by specifying non-designable elements are often introduced. In this study, both strain energy densities in the static stress analysis and the eigenvalue analysis are considered by introducing a connectivity coefficient to ensure an effective load-path for optimal topology.

In the present study, linear buckling optimization will be conducted to maximize critical buckling load factor for a thin-walled structure subjected to either compressive forces or prescribed compressive displacements. Section 2 provides basic formulations for buckling optimization with new constraints on the load-path continuity and the lower bound of the objective function. Section 3 presents the novel response

functions, MIST algorithm (Tong and Lin 2011; Vasista and Tong 2012) and implementation in MSC NASTRAN (MSC.Software 2011). In Section 4, numerical results are presented for optimization of in-plane and out-of-plane buckling of a plate. In Section 5, influences of the soft materials on the critical buckling loads are investigated.

2 Problem definitions of finite element based optimization for buckling loads

2.1 Brief overview of MIST

MIST (Tong and Lin 2011; Vasista and Tong 2012) involves sequentially finding approximate solutions for optimization based on structural responses obtained in the previous iterations, where features of SIMP, ESO and LSM are combined, i.e., material representation in SIMP (Bendsoe and Kikuchi 1988; Zhou and Rozvany 1991; Rozvany et al. 1992), non-explicit sensitivity analysis in ESO (Xie and Steven 1993; Querin et al. 1998) and implicit boundary expression in LSM (Sethian and Wiegmann 2000; Wang et al. 2003; Yamada et al. 2010).

The topology optimization problem in MIST can be formulated in a simple form as to find the optimum iso-surface threshold t:

$$\textit{Maximize}: \quad J(t) = \int_{\Omega} \Phi(u) H(t, \Phi(u)) d\Omega \tag{1a}$$

$$\textit{Subject to}: \textit{Governing equations and boundary conditions for system response } u \tag{1b}$$

$$\int_{\Omega} H(t, \Phi(u)) d\Omega - V_f V \le 0$$

where J is the objective function; u represents a spatial response of the system, $\Phi(u)$ is a measure of system responses in the design domain and is referred to as a response function; Ω represents the design domain dependent of t, t denotes an iso-surface threshold level, $H(t,\Phi(x))=1\,\forall x \in \{\Phi(x) \ge t\}$ or $H(t,\Phi(x))=0\,\forall x \in \{\Phi(x) < t\}$ is the Heaviside function that defines solid or void for every points in the design domain. This means that a domain with $\Phi(u)$ function above the iso-surface threshold level t is solid and that below it is void. V and V_f represent the total volume of the design domain and the desired volume fraction. Evidently, one of the key steps in MIST is to choose an efficient and appropriate response function $\Phi(u)$. When it properly selected, optimal topology for an objective function can be obtained (Tong and Lin 2011).

In essence, the MIST algorithm finds solution of the above problem in a nested iterative process. In each iteration, for a response function $\Phi(u)$ calculated from the system response using the design domain $\Omega(t^k)$ of the previous iteration (or an initial guess in case of the first iteration), an update t^{k+1} is first calculated by making the material constraint in (1b) binding; a subsequent $\Omega(t^{k+1})$ is determined and scaled by the move limit, and then used to solve for an update in the system response function via solving the governing equations. Details about the MIST implementation will be discussed in Section 3.

2.2 Problem statement

Finite element analysis for structural buckling normally includes two analysis steps (Cook et al. 2001): 1) static stress analysis using equilibrium equations to generate stress distributions caused by applied loadings; 2) mode analysis using eigenvalue equations defined by the stiffness matrix and geometric stiffness matrix (GSM) to find eigenvalues and eigenvectors. Critical loads or displacements for structural buckling are obtained via multiplying the obtained eigenvalues by the appropriate applied loads or displacements.

When stiffness matrix and GSM are symmetrically-positive definite, $\lambda_1>0$ and it can be expressed as (Cook et al. 2001):

$$\lambda_1 = \frac{\{\mathbf{Y_1}\}^T[\mathbf{K}]\{\mathbf{Y_1}\}}{\{\mathbf{Y_1}\}^T[\mathbf{K_\sigma}]\{\mathbf{Y_1}\}} = \frac{k_1}{k_{\sigma 1}} = \frac{2}{k_{\sigma 1}} E_\lambda = \frac{2k_1}{k_{\sigma 1}^2} E_\sigma \tag{2}$$

where λ_1 is the 1st order eigenvalue for structural buckling; $[\mathbf{K}]$ is the stiffness matrix; $[\mathbf{Y_1}]$ is the eigenvector for λ_1; $[\mathbf{K_\sigma}]$ is the geometric stiffness matrix (GSM), which relies on geometry, element types and applied loadings (Cook et al. 2001); k_1 and $k_{\sigma 1}$ are the generalized stiffness and geometric-stiffness for the 1st order mode; E_λ and E_σ are the total strain energies associated with the stiffness matrix and the GSM for the 1st order mode. During buckling, energies E_λ and E_σ are exchanged (Cook et al. 2001). In iterative processes, the GSM will be not positive definite when localized tensile modes appear (see Table 1 in Section 4.5). In buckling optimization, it is meaningful only when $k_{\sigma 1}>0$.

Equation (2) can be used to establish relationships between eigenvalue λ_1 and physical response functions. In the existing buckling optimization, a response function based on E_λ used to maximize λ_1 or that based on E_σ used to minimize $(1/\lambda_1)$ is normally used (Neves et al. 1995, 2002; Bendsoe and Sigmund 2003). When an eigenvector is scaled to create a unit value of the generalized stiffness ($k_1=1$) or geometric

Table 1 Eigenvalues of a column-beam (600×100×4; α=0; V_f=0.5) at iterations 118–121 when λ_{min} is not specified

Eigenvalue order	Iteration 118	Iteration 119	Iteration 120	Iteration 121
λ_1	−2.09855	−2.09856	−2.09858	−2.09857
λ_2	−3.03510	−3.03512	−3.03512	−3.03511
λ_3	−3.73411	−3.73411	−3.73412	−3.73411
λ_4	−3.73982	−3.73985	−3.73986	−3.73985
λ_5	3.977548	3.977547	3.977547	3.977547
λ_6	3.977555	3.977550	3.977566	3.977564
$(\lambda_6 - \lambda_5)/\lambda_5$	1.76×10^{-6}	7.54×10^{-7}	4.78×10^{-6}	4.27×10^{-6}

stiffness ($k_{\sigma 1}$=1), relationships of eigenvalue λ_1 and E_σ or E_λ are directly established.

When the response function E_σ or E_λ is used for some structural optimizations such as plate buckling optimization, reinforcements by specifying solid elements are often used to obtain optimal structural designs with effective load-path (Neves et al. 1995; Bendsoe and Sigmund 2003; Pedersen and Nielsen 2003). It is noted that there is another part of strain energy in finite element (FE) buckling analysis, i.e., strain energy E_s (=0.5$\{\mathbf{u}\}^T[\mathbf{K}]\{\mathbf{u}\}$) in static stress analysis, which may be used to model load-path continuity.

Based on (2), an expression of λ_1 is given by:

$$\lambda_1 = \frac{2}{\alpha_1+\alpha_2}\left(\frac{\alpha_1}{k_{\sigma 1}}\int_\Omega E_{\lambda d}d\Omega + \frac{\alpha_2 k_1}{k_{\sigma 1}^2}\int_\Omega E_{\sigma d}d\Omega\right) + \alpha_3\left(\int_\Omega E_{\lambda d}d\Omega - E_\lambda\right) + \alpha_4\left(\int_\Omega E_{sd}d\Omega - E_s\right) \quad (3a)$$

where α_1, α_2, α_3 and α_4 are real numbers and $\alpha_1+\alpha_2\neq 0$, which should be chosen by user. Apparently, the simplest case is: α_1=1 and $\alpha_2=\alpha_3=\alpha_4$=0; the Φ function for this case can be used in optimization to maximize the buckling load of plane structures. However, such a choice is not ideal for plate buckling problems owing to creation of disjointed structural components. Equation (3a) can be rewritten as:

$$\lambda_1 = \left[\frac{2\alpha_1}{(\alpha_1+\alpha_2)k_{\sigma 1}}+\alpha_3\right]\int_\Omega E_{\lambda d}d\Omega + \alpha_4\int_\Omega E_{sd}d\Omega + \left[\frac{2\alpha_2\quad k_1}{\alpha_1+\alpha_2 k_{\sigma 1}^2}E_\sigma - (\alpha_3 E_\lambda + \alpha_4 E_s)\right] \quad (3b)$$

In an iterative process, the 3rd term on the right hand side of (3b) is a real number calculated by the previous iterations. It will not change shapes of the Φ function surface and can be equal to zero for a special combination of α_1, α_2, α_3 and α_4. Therefore, λ_1 can be expressed as:

$$\lambda_1 = \int_\Omega\left\{\left[\frac{2\alpha_1}{(\alpha_1+\alpha_2)k_{\sigma 1}}+\alpha_3\right]E_{\lambda d} + \alpha_4 E_{sd}\right\}H(t,\Phi)d\Omega \quad (3c)$$

Equation (3c) indicates that the response function can be expressed by a linear combination of strain energy densities in the two FEA steps. Selection of coefficients should ensure that λ_1>0. Equation (3c) can be rewritten as:

$$\lambda_1 = \alpha_4\int_\Omega\left[\frac{(1-\alpha)}{\alpha}E_{\lambda d} + E_{sd}\right]H(t,\Phi)d\Omega \quad (3d)$$

where

$$\frac{(1-\alpha)}{\alpha} = \frac{1}{\alpha_4}\left[\frac{2\alpha_1}{(\alpha_1+\alpha_2)k_{\sigma 1}}+\alpha_3\right] \quad (3e)$$

It is worth noting that the terms in brackets of the last two terms in (3a) are zero. This allows inclusion of the distributions of $E_{\lambda d}$ and E_{sd} in the response function as in (3c), which is demonstrated to be beneficial if chosen properly in terms of finding practical optimum structural topologies and implicitly optimizing the objective value.

On the basis of above discussions, finite element based buckling optimization to maximize eigenvalue λ_1 can be stated as:

$$\textit{Maximize}: \quad \lambda_1 \quad (4a)$$

$$\textit{Subject to}: \begin{cases} [\mathbf{K}(\mathbf{x_e})]\{\mathbf{u}\} = \{\mathbf{F}\} \\ ([\mathbf{K}(\mathbf{x_e})] - \lambda[\mathbf{K_\sigma}(\mathbf{x_e},\mathbf{u})])\{\mathbf{Y}\} = 0 \\ 0 < \lambda_{\min} < \lambda_1 \\ \text{load-path continuity of topology} \\ \sum_{e=1}^{N_e}(x_e V_e) \leq \quad V_f V \\ 0 < x_{\min} \leq x_e \leq 1 \end{cases} \quad (4b)$$

where $\{\mathbf{F}\}$ is the force vector; $\{\mathbf{u}\}$ is the displacement vector in static analysis; $\{\mathbf{Y}\}$ denotes the eigenvector; $\lambda_{\min}$ is the lower bound of eigenvalue λ_1; V_e is the element volume; N_e is the element number; x_e is the design variable for the e^{th} element ranging from 0 to 1, which characterizes the use of material at an element level; and $x_{\min}$ its minimum value to prevent matrix singularity.

In an iterative process, stiffness is assembled by: $[\mathbf{K}] = \sum_{e=1}^{N_e} x_e^p[\mathbf{k_e}]$ where $[\mathbf{k_e}]$ is the stiffness matrix for the e^{th} element with full solid materials; p is the penalty. In a two-dimensional

design problem, p=3 for the applied forces. When a structure is subjected to the enforced displacements $\{\mathbf{u_d}\}$, it is equivalent to the case of an applied force $\{\mathbf{F_d}\}=[\mathbf{K_d}(\mathbf{x_e})]\{\mathbf{u_d}\}$, where $[\mathbf{K_d}(\mathbf{x_e})]$ is the stiffness for $\{\mathbf{u_d}\}$. If $p>1$, $\{\mathbf{F_d}\}$ will be decreased by the penalty and the effect of $\{\mathbf{u_d}\}$ will be inaccurately accounted for. Therefore, p=1 is used for the enforced displacements.

In (4b), the constraint of $0<\lambda_{\min}<\lambda_1$ is used to eliminate the spurious local buckling mode shapes. $\lambda_{\min}$ should be large enough to prevent the spurious mode shape output in FEA but smaller than the real 1st order eigenvalue that may appear in iterations. In the present computation, $\lambda_{\min}=10^{-3}$, which is around $0.001\lambda_1$. The constraint of load-path continuity is realized by introducing a connectivity coefficient in the present study to ensure that the structure with an optimum topology has the load-bearing capacity.

3 Response function, algorithm and implementation of MIST for buckling analysis

3.1 Formulation of the response function Φ

Based on (1)-(4), the Φ function for maximizing eigenvalue λ_1 may be constructed by using nodal values of $E_{\lambda d}$, $E_{\sigma d}$ or their proper combination plus E_{sd} to obtain effective load-path. In the present computation, $E_{\lambda d}$ and E_{sd} are used to construct the Φ function as they can be directly obtained in the two FEA steps. It can be derived by comparing (1b) and (3d):

$$\Phi = (1-\alpha)E_{\lambda d} + \alpha E_{sd} = (1-\alpha)\Phi_\lambda + \alpha\Phi_s \tag{5}$$

where Φ_s and Φ_λ are the response functions for the static stress analysis and the buckling analysis for mode 1 and they are constructed by using the nodal values of strain energy densities in the two steps; α is referred to as the connectivity coefficient.

When α=0, the response function is the same as that used in most of the existing literatures and when α is too large, strain energy in static stress analysis will dominate iteration process leading to topologies for non-buckling problems. On the basis of (2), when an eigenvector for the 1st order mode is scaled to result in $k_{\sigma 1}$=1, the strain energy in the eigenvalue analysis step is given by: $E_\lambda=\lambda/2$ and that can also be expressed as $E_\sigma=k_\sigma^2\lambda/2$ when the eigenvector is scaled to generate k_1=1. In the present computation, the case of $k_{\sigma 1}$=1 is considered and thus the response function in (5) is used. In MIST, nodal values of the physical response function are used to construct the Φ function surface, which can be extracted from values at Gaussian points or element centres, see Appendix A.

The novel formulation (5) indicates that the response function associated to eigenvalue λ_1 can be approximately expressed as a linear combination of strain energy densities based on Φ_s and Φ_λ functions. In the existing literatures on topology optimization for buckling analysis, strain energy density based on Φ_λ is mainly used, which is a special case of (5) with no connectivity coefficient (α=0).

It is seen that the response function defined in (5) is directly related to an objective function to maximize the critical load where the connectivity coefficient is used to take into account effective load-paths. Once the response function is selected, buckling optimization can be conducted by using the MIST algorithm as described in Section 3.2.

3.2 Basic algorithm

In MIST (Tong and Lin 2011; Vasista and Tong 2012), iso-surface of the chosen response function Φ is sought to define the structural boundary by meeting the volume constraint and also minimizing or maximizing an objective function (Tong and Lin 2011; Vasista and Tong 2012). The algorithm based on the finite element analysis can be described as follows:

Step 1 Initialization

The initialization mainly includes two sets of input data. One contains all necessary data for finite element analysis in a design domain and the other requires selection of initial values of the weighting factors x_e (e = 1, 2, …, N_e) for all elements with reference to the volume constraint. This is similar to element based material density variables used in SIMP. A uniform material distribution is often assumed as in (Tong and Lin 2011; Vasista and Tong 2012). Other initial parameters such as a volume constraint, penalty, move limit and a filter radius are also specified in this step.

Step 2 Finite element analysis

In finite element analysis (FEA), the material properties for each element are calculated based on initial or updated weighting factors by using an appropriate material model in SIMP and the other input data are not changed. An input data file for the FEA is then created in the 1st iteration or modified in subsequent iterations by using the initial/updated weighting factors and the other data required for FEA. In the FEA input file, $\lambda_{\min}$ (e.g., 10^{-3}) is specified. By using the initialized or updated input data file, FEA can be conducted and an output data file containing information on displacements, strains and stresses is generated. In this paper, MSC NASTRAN is used as an FEA solver. Interfaces and input/output data files will be discussed in details in Section 3.3.

Step 3 Construction of the Φ function

1) Nodal value calculation

The surface of the chosen Φ function for two-dimensional analysis can be constructed by the calculated Φ values (as z coordinate) at nodes (located by its x and y coordinates in Cartesian coordinate system) by using the FEA results of the initial or previous iteration. In the FEA output data, physical responses, such as stress, strain and strain energy density, may be given at Gauss points, element centers or nodes. If physical responses are output at nodes, they are directly used to form the Φ function surface. When the physical quantities are output at Gauss points, the Φ function surface can be constructed by evaluating their nodal values through averaging the values at the surrounding Gauss points (Tong and Lin 2011; Vasista and Tong 2012). When the responses are output at element centers, their node values can be calculated by the 2nd order polynomial interpolation and this method will be used in this paper.

As the 4-node isotropic elements are used, strain energy density is a 2nd order polynomial function with respect to coordinates x and y and thus the Φ function is the 2nd order surface. Consider 3 adjacent elements with the unit length in x direction. When the strain energy densities are output at element centers (x=0, ±1), values at the edge centers (x=±0.5, ±1.5) can be calculated by using:

$$\Phi = \Phi(0) + \frac{1}{2}[\Phi(1)-\Phi(-1)]x + \left\{\frac{1}{2}[\Phi(1)+\Phi(-1)]-\Phi(0)\right\}x^2 \quad (-1.5\le x\le 1.5) \tag{6a}$$

When element edges locate in the middle of a design domain, two or three values at one point are averaged. By replacing x with y in (6a) and using the data of the element edge centers, the nodal values can be obtained.

2) Filtering

Topology optimization can be mesh dependent (Sigmund and Petersson 1998). To solve this issue, filtering element sensitivity could be used for gradient-based topology optimization (Sigmund and Petersson 1998; Bendsoe and Sigmund 2003). This method is purely heuristic although it produces results similar to the local gradient constrained method (Sigmund and Petersson 1998; Bendsoe and Sigmund 2003) where the sensitivity of a specific element is modified based on a weighted average of the element sensitivities within a fixed spatial neighbourhood or filtering radius. In MIST (Tong and Lin 2011; Vasista and Tong 2012), the Φ function can be filtered similarly by using (Vasista and Tong 2012):

$$\overline{\Phi}_j = \frac{\sum_{i=1}^{N_i} w_i \Phi_i}{\sum_{i=1}^{N_k} w_i} \quad where\, w_i = 1-\frac{r_{ji}}{r_{\min}} \tag{6b}$$

where, $r_{\min}$ is the filter radius, r_{ji} is the distance between nodes j and i; N_i is the node number in the circle centered at node j with a radius of $r_{\min}$. In general, $r_{\min}$=(1.5~2.5)l where l is the element length (Sigmund and Petersson 1998; Vasista and Tong 2012).

3) Normalization

To easily calculate the iso-surface threshold level t, the Φ function will be normalized by:

$$\overline{\Phi} = \frac{\Phi-\Phi_m}{\Phi_a} \quad where \tag{6c}$$

$$\Phi_m = \frac{1}{2}[\max\{\Phi\} + \min\{\Phi\}];$$

$$\Phi_a = \frac{1}{2}[\max\{\Phi\}-\min\{\Phi\}]$$

After normalization, $-1\le \overline{\Phi} \le 1$.

Step 4 Update of weighting factors

1) Incremental direction of the weighting factors

For the cases of very flat or steep Φ function surface, the level t can be difficult to find. In the present computation, an efficient algorithm is developed: 1) t_n ($-1<t_n<1$) is simply calculated by counting the node numbers for the prescribed volume constraint; 2) t_n may be the iso-surface threshold level to be found for the fine mesh and otherwise t is calculated using an iterative bisection method by considering the volume constraints (Tong and Lin 2011; Vasista and Tong 2012) in a range of (t_n - ε)< t<(t_n+ε) (tolerance ε=0.01). Weighting factor x_e equal to 1 represents the use of solid material if all of its nodal Φ values of the e^{th} element are above the iso-surface, and x_e equal to or close to zero denotes the use of void material if all nodal Φ values of this element are below the iso-surface. When some nodal Φ values of the e^{th} element are above and the others are below the iso-surface, its weighting factor is defined as the fraction of the project area above the iso-surface to the element total area. The project area is the one enclosed by the boundary and element edges; in the present computation, a curve of the boundary is approximated by a straight line and the polygonal

area is calculated. When the iso-surface level or threshold value is found, weighting factors $\{\mathbf{x}_e\}_k$ are obtained and incremental direction $\Delta\{\mathbf{x}_e\}_k=\{\mathbf{x}_e\}_k-\{\mathbf{x}_e\}_{k-1}$ at the k^{th} iteration is determined.

2) Incremental magnitude of the weighting factors

Generally, $\{\mathbf{x}_e\}_k$ should not be directly used for FEA at the next iterative step (Tong and Lin 2011; Vasista and Tong 2012) owing to unstable or divergent iterations and thus move limit is introduced to reduce increments, similar to the move limit used in optimality criteria (Bendsoe and Kikuchi 1988). Constant or variable move limit may be used. In this study, the dynamic move limit in (Vasista and Tong 2012) is used, where the move limit is halved when the objective function starts to oscillate.

In an iterative process, the weighing factors x_e ($e=1, 2, \ldots, N_e$) must be in the range of ($0<x_{\min}\le x_e\le 1$) to avoid possible numerical singularity ($x_e<x_{\min}$) and unacceptable design ($x_e>1$). Therefore, the updating scheme for the weighting factors is defined as:

$$\Delta\{\mathbf{x}_e\}_k = \{\mathbf{x}_e\}_k^{(1)}-\{\mathbf{x}_e\}_{(k-1)} \tag{7a}$$

$$\{\mathbf{x}_e\}_k^{(2)} = \{\mathbf{x}_e\}_{(k-1)} + k_{mv}\{\Delta\mathbf{x}_e\}_k \tag{7b}$$

$$\begin{aligned}\{\mathbf{x}_e\}_k^{(3)} &= \max\left\{\{\mathbf{x}_e\}_k^{(2)}, x_{\min}\right\} \text{ and } \{\mathbf{x}_e\}_k^{(3)} \\ &= \min\left\{\{\mathbf{x}_e\}_k^{(2)}, 1\right\}\end{aligned} \tag{7c}$$

where k_{mv} is the move limit, $0<k_{mv}\le 1$; $\{\mathbf{x}_e\}_k^{(3)}$ are the updated weighting factors used for the next iteration. It is noted that, similar to SIMP, one element is also depicted by one variable (x_e) in MIST and the design variables are updated by using (7a)-(7c).

In the SIMP, penalty (=3) greater than 1 is used to penalize intermediate densities to obtain an almost black and white design that can be easily manufactured. This approach is also employed in the MIST. Although the topology is represented by the implicit boundary or intersection of the iso-surface and the Φ function surface in the MIST element based design variables are used in FEA and updated via (7a)-(7c).

Step 5 Convergence test

Convergence parameters may be defined in terms of the changes in the weighting factors, objective function and the response surface at element or overall domain level. The weighing factors $\{\mathbf{x_e}\}$, topology, eigenvalues, the Φ function and iso-surface are tracked at each iterative step. The iterative process may be deemed as convergent when one or more parameters of these physical quantities are less than tolerances. Setting the convergent tolerances is normally problem-dependent and the maximum iterative number (e.g., 200) can also be set to avoid the iteration without ending. In the present computations, both $\Delta t^k=|t^k-t^{k-1}|\le 0.001$ and $\Delta\lambda_1^k=|\lambda_1^k-\lambda_1^{k-1}|/\lambda_1^k\le 0.1\%$ are chosen as the convergent criteria and 200 is the maximum iterative number.

When the convergence criteria are met, the iterations terminate or otherwise go to **Step 2**.

3.3 Implementation in commercial FEA software

In this study, finite element analysis is conducted by using NASTRAN. Interface with this FEA software allows automatic generation or modification of the input data file for NASTRAN and reading of the output data file from NAST RAN. The details are given in Appendix B.

Strain energy densities at each element center in the two steps can be directly read from the NASTRAN output file. By using the 2nd order polynomial interpolation technique, their nodal values can be found and then the Φ function are constructed by filtering (Vasista and Tong 2012) and normalizing these data. By calculating the iso-surface threshold level t, the weighting factors $\{\mathbf{x}_e\}_k^{(1)}$ can be obtained and the new weighting factors $\{\mathbf{x}_e\}_k^{(3)}$ are calculated by using (7a)-(7c). An iterative process continues by using the updated weighting factors until convergence criteria are met.

4 Numerical results and discussion

By using the present formulation for buckling analysis and MIST, topology optimization will be presented for a plate subjected to uniformly-distributed force and enforced displacement as shown in Fig. 1a and a column-beam subjected to force(s) in Fig. 1b. The material properties and thickness for

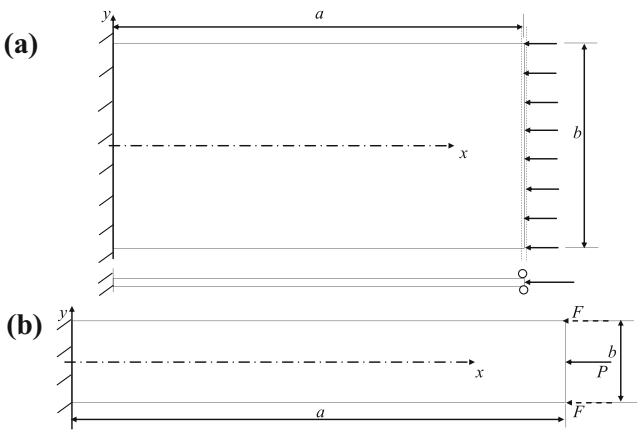

Fig. 1 Samples for buckling analysis (**a**) a clamped plate subjected to the distributed force or enforced displacement; (**b**) a column-beam subjected to concentrated force P or F

the two structures are: E=70 (GPa), ν=0.3 and t=4 (mm). The column-beam structure deforms in-plane only and plane stress state is assumed. In all computations, $\lambda_{\min}=10^{-3}$ is specified.

4.1 MIST Implementation

In the present computations of Sections 4.1 and 4.2, uniformly distributed loading is applied to the right end of a plate (a= 400 mm, b=200 mm) and the resultant force is P=4 (kN). It is noted that magnitude of the applied loading affects increment magnitude in an iterative process. When eigenvalue λ_1 is found, the critical load is given by $P_{cr}=\lambda_1 P$.

Figures 2, 3 and 4 illustrate iterative processes of topology optimization using MIST to maximize buckling loading of the plate in Fig. 1a. In the present computation using NASTRAN, 4-node isotropic shell element CQUAD4 is used, which is based on the 1st order shear deformation theory. The mesh scheme of (80×40) is used for Figs. 2, 3 and 4. The connectivity coefficient and the volume constraint are α=0.1 and V_f=0.5.

Figure 2a-d show the Φ function surface and the threshold iso-surface at iterations 1, 10, 30 and 200. Figure 3a-d show topologies at these iterative steps and Fig. 3d is the optimal topology for the maximum critical buckling load. Figure 3b-d show that topology at iteration 30 is very close to that at iteration 200.

In the iterative computations, eigenvalues versus iteration are plotted in Fig. 4, which indicates that the 1st –5th order eigenvalues are convergent. At iteration 1, 10, 30 and 60~200, the 1st order eigenvalue is 0.611, 3.62, 4.42 and 4.42. It is seen that the converged eigenvalue is reached at the 60th iterative step and the converged value is 90.4 % as large as that of this plate with full solid material. It is noted that the 1st order eigenvalue of this solid plate computed by the FEA with a mesh of (40×80) using NASTRAN is 4.885. This example shows that a 50 % reduction in material use yields decrease of 10 % in buckling load.

4.2 Influences of mesh and connectivity coefficients

Figures 2, 3 and 4 show that the present formulations and algorithms are capable of conducting topology optimization to maximize eigenvalue λ_1 for plate buckling. In this section, influences of meshes and connectivity coefficients on the maximum eigenvalue λ_1 of the plate will be investigated to further verify effectiveness of the present formulation and MIST for buckling analysis.

4.2.1 Optimal topologies and eigenvalues for different meshes

In Section 4.1, 4-node isoparametric shell elements are used and the mesh scheme is (80×40). When meshes using the

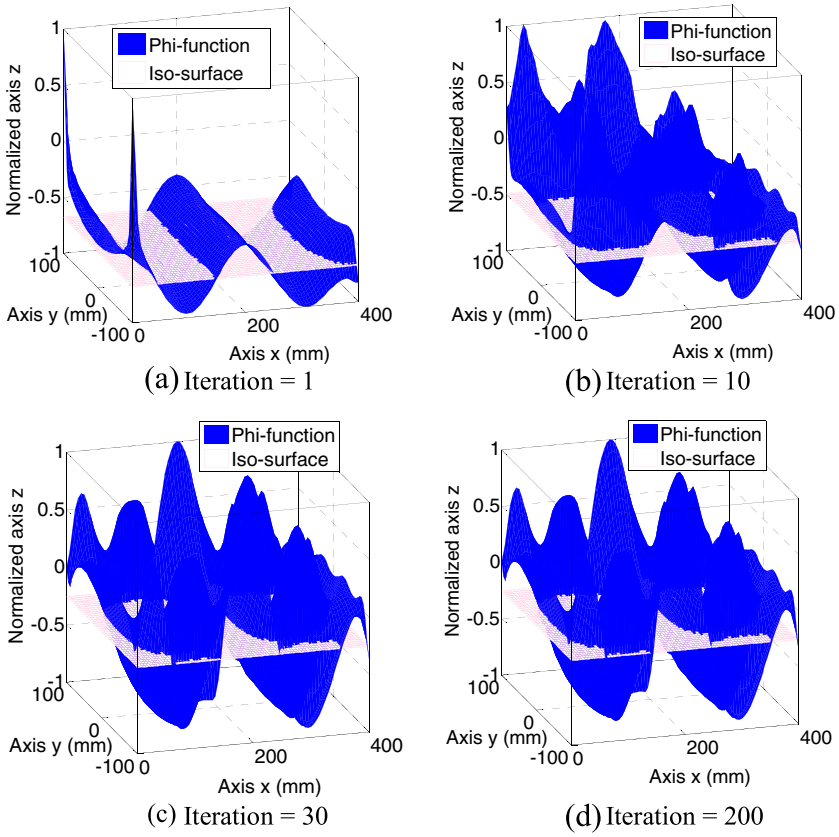

Fig. 2 The Φ function surface and the iso-value surface to maximize λ_1 at iterations 1, 10, 30 and 200

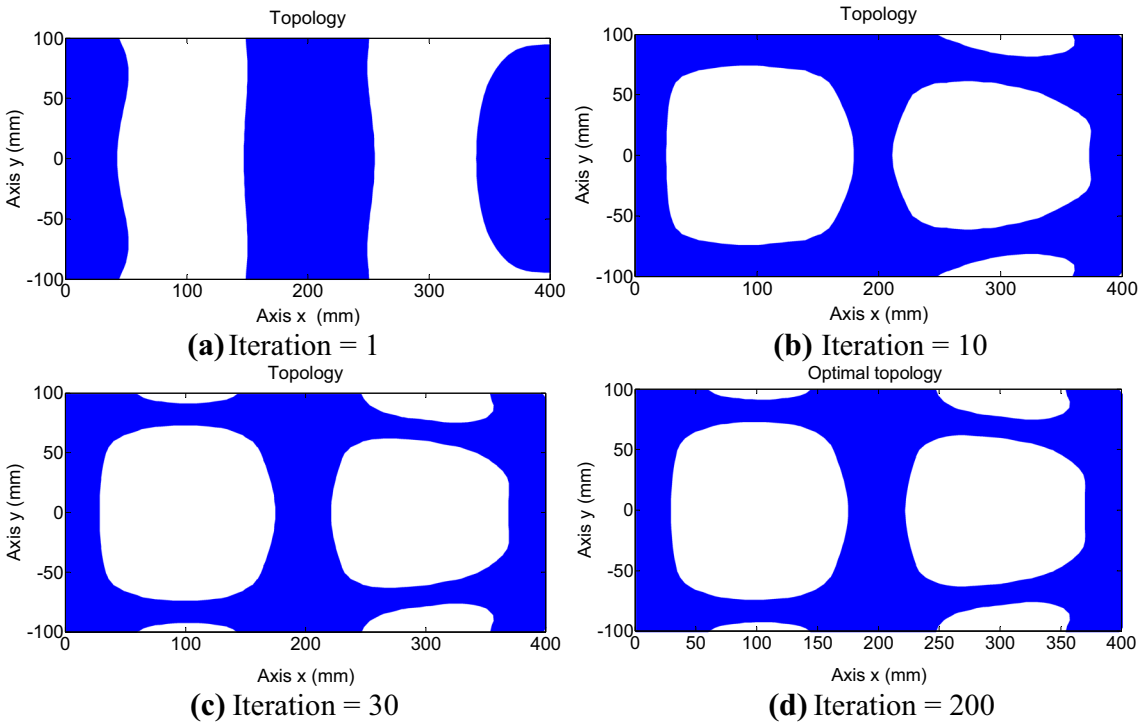

Fig. 3 Topologies to maximize λ_1 at iterations 1, 10, 30 and 200 (mesh: 80×40)

same 4-node element are (40×20), (60×30), (100×50) and (120×60), the optimal topologies are obtained as in Fig. 5a-d. Curves of eigenvalue versus iteration for these cases are almost the same that of Fig. 4 and thus are not given.

When there is no material removal in this plate, the eigenvalues (λ_1) for 5 mesh schemes of (40×20)–(120×60) are: 4.894, 4.888, 4.885, 4.884 and 4.883. It can be deemed that the convergent eigenvalue is achieved by using the mesh of (80×40) whose eigenvalue λ_1 is 0.04 % larger than that for the mesh of (120×60). In the iterative process to maximize λ_1 with α=0.1 and V_f=0.5, the converged values of eigenvalue λ_1 are 4.535, 4.491, 4.423, 4.507 and 4.456 for the 5 mesh schemes, respectively; the difference between meshes (80×40) and (120×60) is 0.74 %. Therefore, the mesh scheme of (80×40) will be used for the plate with a size of (400×200×4 mm^3) in the subsequent computations.

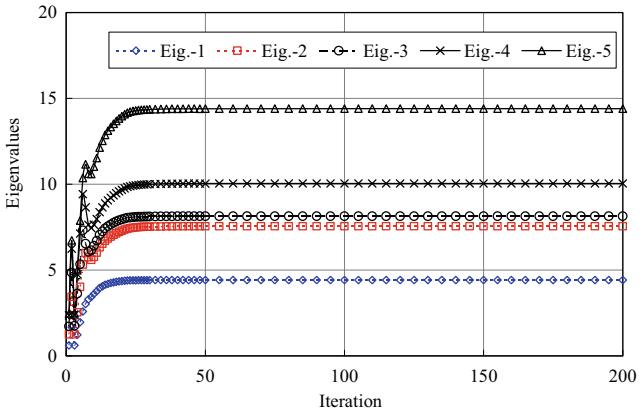

Fig. 4 Eigenvalue versus iteration for a fixed-clamped plate subjected to uniformly distributed compressive forces in buckling optimization (mesh: 80×40)

4.2.2 Optimal topologies for different connectivity coefficients

In the present computation for plate buckling analysis, strain energy densities in the two steps of FEA are considered. The strain energy density for eigenvalue analysis is used to establish relationships between eigenvalue and the response function and the strain energy for the static stress analysis is used for connecting isolated parts to form optimal designs with effective load-path.

In conventional topology optimization for buckling analysis of plate and shell structures, non-designable elements or reinforcements are often specified to obtain load-path continuity designs. In this paper, the Φ function in terms of strain energy densities in the two steps is derived and the reinforcement strategy is not used. In the present formulations, roles and influences of the strain energy density in static stress analysis are reflected by connectivity coefficient α. Applicable ranges of connectivity coefficients will be studied for volume constraints of V_f=0.75 and 0.5 as follows.

Figure 6 illustrates the converged 1st order eigenvalue versus connectivity coefficient when the volume constraints are equal to 0.5 and 0.75, respectively. When different connectivity coefficients are selected, optimal topologies to maximize the 1st order eigenvalue may also be different, as plotted in Figs. 7 and 8.

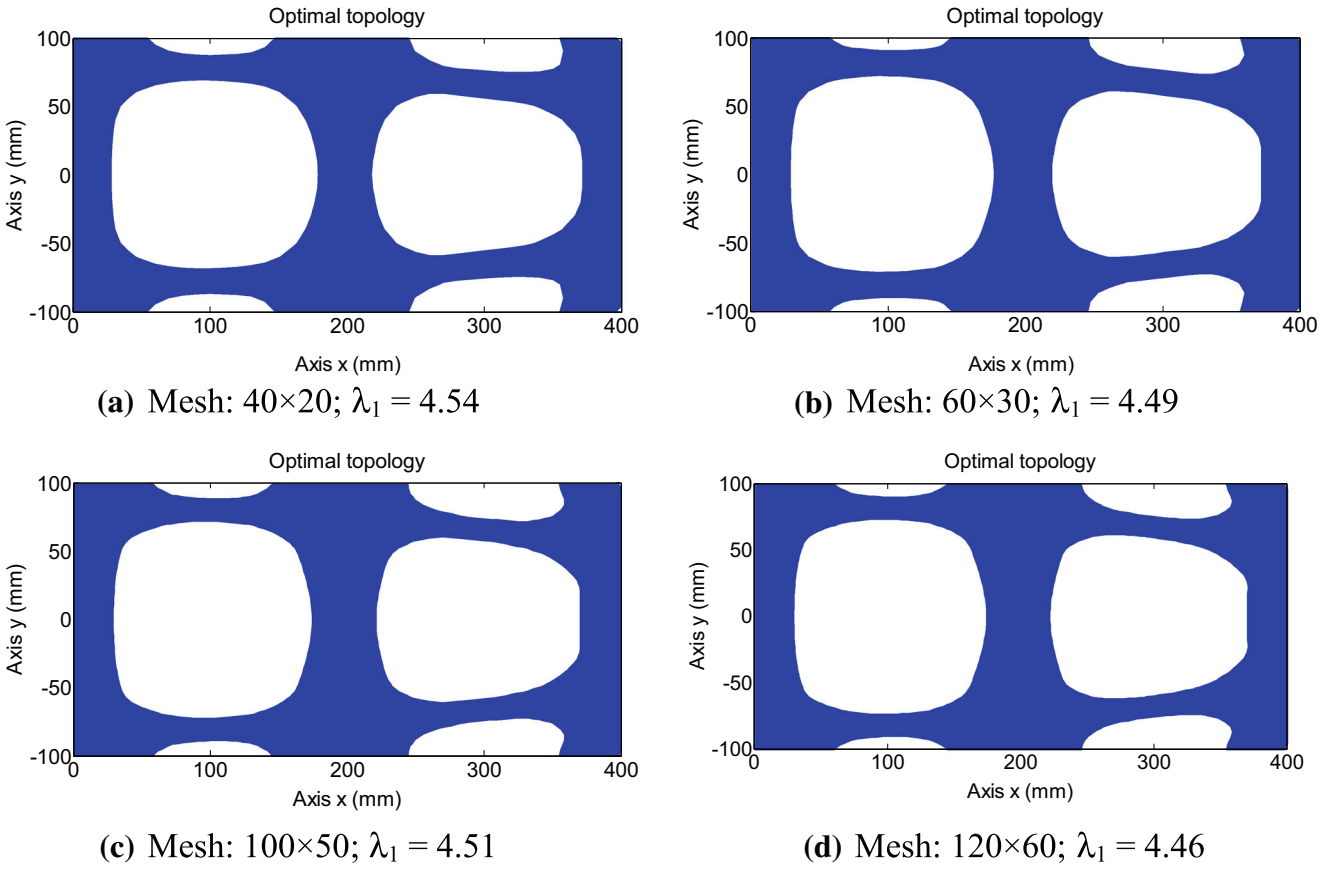

Fig. 5 Optimal topologies of a fixed-clamped plate obtained by using mesh schemes of (40×20)~(120×60) for maximizing buckling loading

Figure 7a-d illustrate optimal topologies of the plate with V_f=0.5 for α=0.04, 0.18, 0.19 and 0.21. When α=0.04~0.18, patterns of the topology are similar as shown in Fig. 7a and b. The topology is changed when $\alpha \geq 0.19$ and larger eigenvalues (λ_1=4.71–4.73) are obtained when α=0.192~0.21. When $\alpha <$ 0.04, the obtained topology lacks effective load-path and when $\alpha > 0.21$, it is a static stress dominated problem. Figure 7e is the material distribution at iteration 100 when α=0, where there exist regions with many grey elements (x_e~ 0.08); the iteration is divergent due to lack of the effective load-path and localized modes. Figure 7f shows the topology when α=0.8; when α=0.6 and 1, almost the same topology and buckling factor as those in Fig. 7f are obtained in the present computations. In this case, optimization is dominated by strain energy density in static analysis and thus the buckling factor is much lower than that shown in Fig. 7a-d. This indicates importance of the connectivity coefficient for load-path continuity of topology.

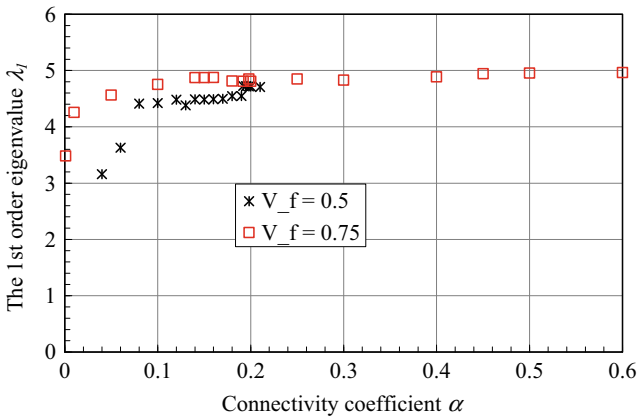

Fig. 6 The 1st order eigenvalue versus coefficient α when V_f=0.5 and 0.75

Figure 8 illustrates optimal topologies of the plate with V_f= 0.75 for α=0.001~0.6. When α varies from 0.001 to 0.25, hole areas in the plate middle region of Fig. 8a decreases and those in the top and bottom edges increases; the optimal topology in Fig. 8a varies to a similar one in Fig. 8b. In a range of α=0.3~0.6, topologies are shown in Fig. 8c-f. Although optimal topologies look quite different for these connectivity coefficients, the converged 1st order eigenvalues are almost the same (λ_1=4.85~4.96) with the maximum difference of 2.39 %. Similarly, when α<0.001, there is no load-path continuity and the problem becomes static stress dominated when α>0.6.

Although the 1st order eigenvalues given by different topologies are almost the same when α=0.3~0.6, the higher

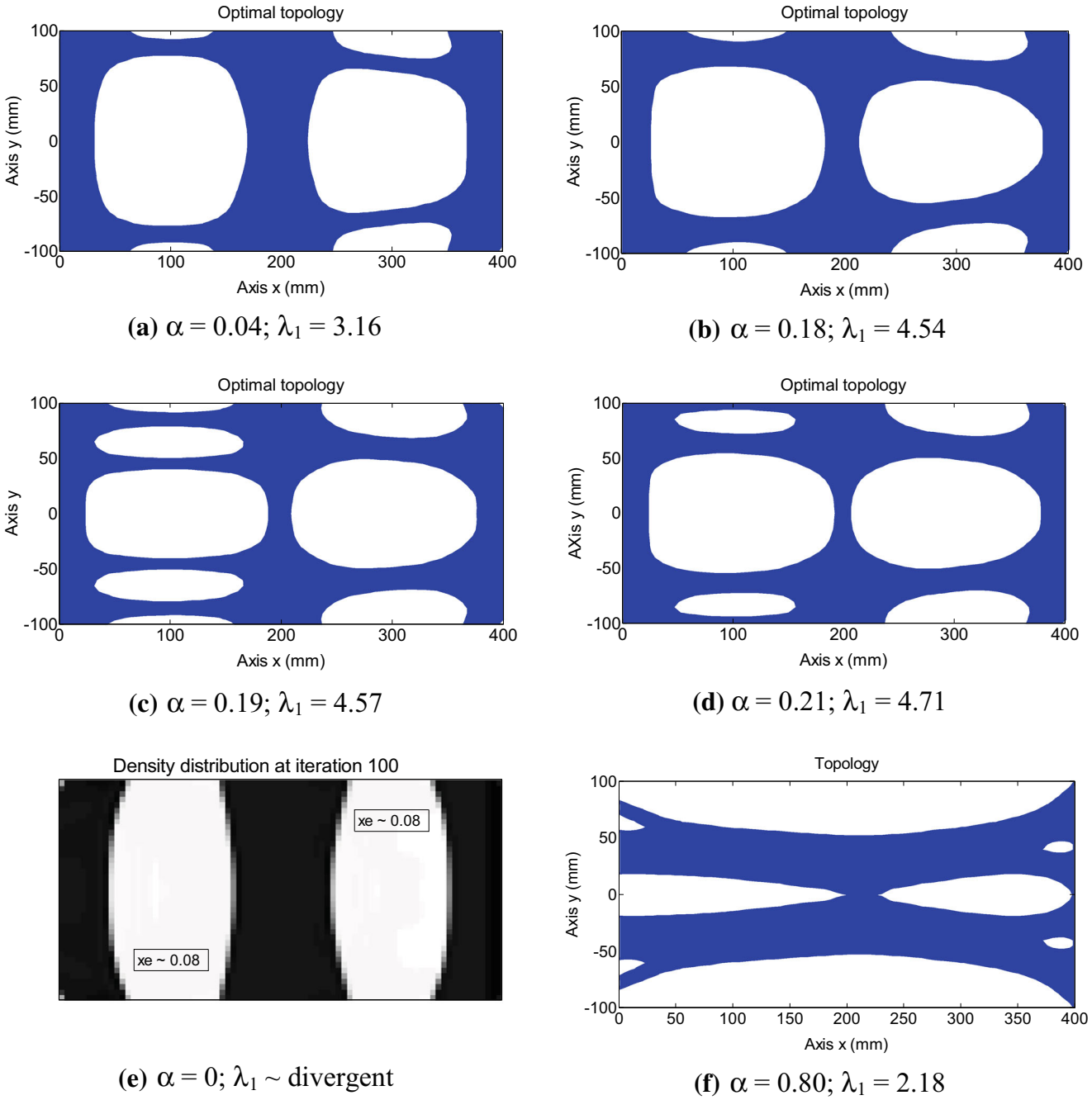

Fig. 7 Optimal topologies for different coefficients when V_f=0.5

order eigenvalues can be different, as shown in Fig. 9. The 1st–3rd order eigenvalues for these connectivity coefficients are plotted in Fig. 9a-d. It is seen that the 3rd order eigenvalue given in Fig. 9b, c) or (d) is much higher than that in Fig. 9a. The convergent eigenvalues are also observed in the four figures.

These examples show that in addition to ensuring the load-path continuity, connectivity coefficient α has a remarkable effect in enhancing the critical buckling load of the optimized structure. When α=0.21 for V_f=0.5, the critical load is reduced by 3.2 %. When α=0.3~0.6 for V_f=0.75, the buckling load hardly decreases.

The coefficients α_1, α_2, α_3 and α_4 introduced in (3a)-(3c) are difficult to determine as these coefficients can have different combinations and thus a trial-and-error method is used. The present numerical results for plate buckling analysis show that: 1) $0<\alpha<1$; 2) when $\alpha<\alpha_{min}$ (= 0.04 for Fig. 7), load-path is discontinuity; $\alpha>\alpha_{max}$ (= 0.21 for Fig. 7), it degenerates to an in-plane compliance problem; 3) a range $[\alpha_{min}, \alpha_{max}]$ of the effective value increases with a volume fraction V_f; 4) the

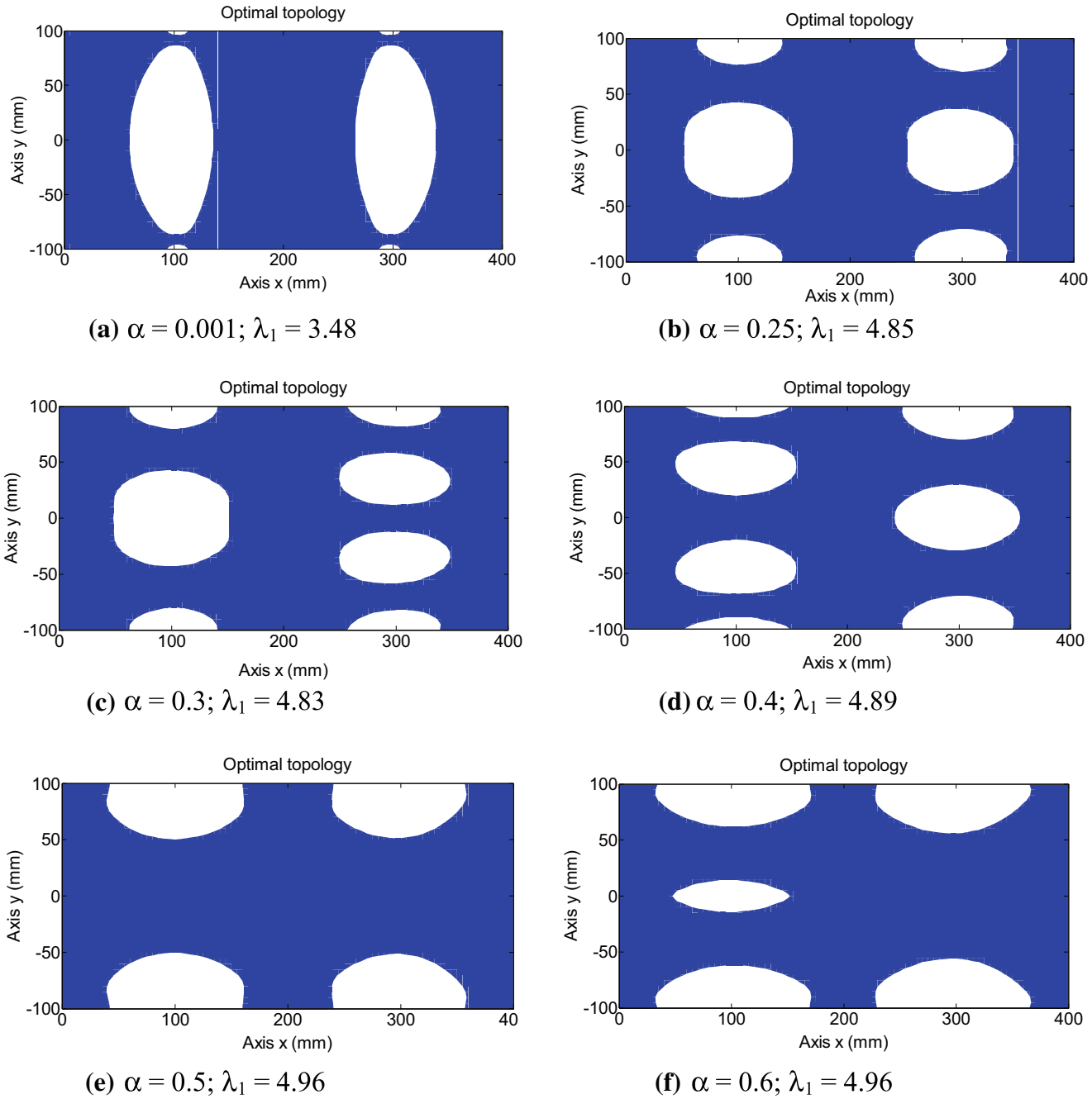

Fig. 8 Optimal topologies and converged eigenvalue λ_1 when α=0.001~0.6 and V_f=0.75

maximum buckling factor (λ_1) increases with α when $\alpha \subset [\alpha_{\min}, \alpha_{\max}]$ as shown in Fig. 6, which could be understood as the in-plane compliance enhances the effective load-path.

4.3 Topology for plate buckling subjected to enforced displacement

In Sections 4.1 and 4.2, the plate is subjected to uniformly distributed load. In this section, optimal designs for a plate in Fig. 1a subjected to the enforced displacement will be studied. In optimization to maximize eigenvalue λ_1 of a plate subjected to an enforcement displacement, penalty should be 1 (p=1 and $x_{min}=10^{-9}$).

Similar to Figs. 6 7, 8 and 9, different topologies and eigenvalues can be obtained for different volume constraints and connectivity coefficients when an enforced displacement is applied to the plate right edge. Figures 10 and 11 illustrate optimal topologies and eigenvalues of the plate subjected to the enforced displacement of −0.2 (mm) for the cases of (V_f= 0.5; α=0.4) and (V_f=0.75; α=0.15), respectively.

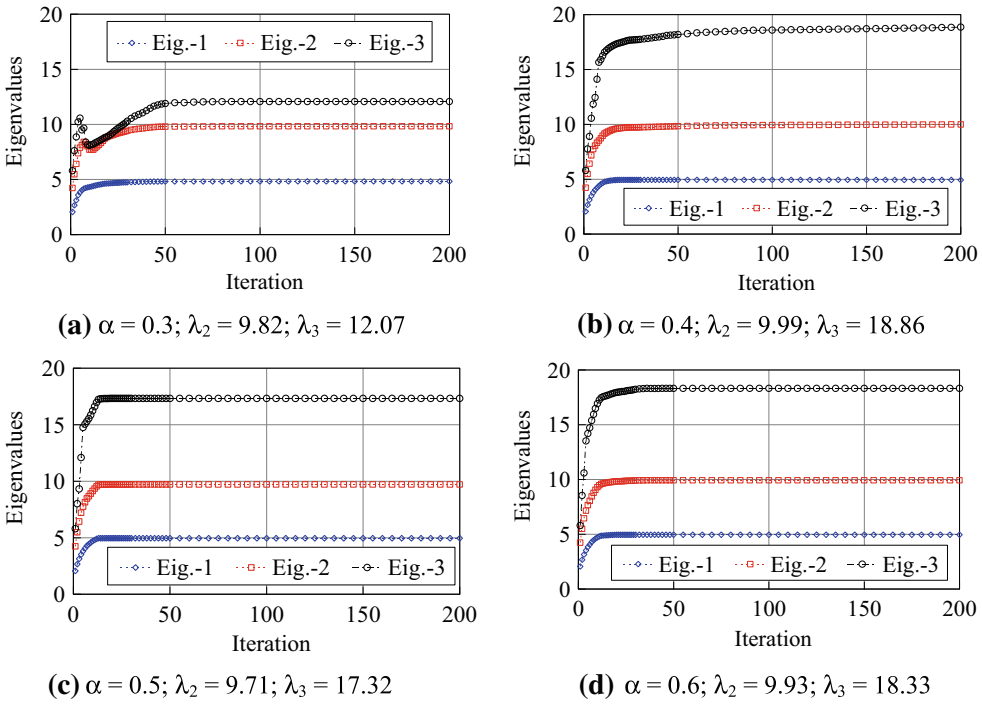

Fig. 9 Eigenvalue versus iteration when α=0.001~0.6 and V_f=0.75

It is seen that the optimal topology in Fig. 10a is similar to that in Fig. 5d but the design in Fig. 10a is symmetrical about x=200 mm. The symmetrical design is also found in Fig. 11a (V_f=0.75 and α=0.15). Figures 10b and 11b indicate that the converged eigenvalues are achieved in these iterative processes and eigenvalues (λ_1) of the optimal designs are significantly increased.

4.4 Optimal buckling design for a relatively-narrow plate and column-beam

By using MIST and the present formulation, optimal designs to maximize buckling forces of relatively-narrow plates and a column-beam shown in Fig. 1b are further investigated; the structure dimensions considered are a=400 and 600 mm, b=100 mm, t=4 mm and the mesh schemes used are (160×40) and (240×40) for both the plate and column-beam. In the column beam as shown in Fig. 1b, two loading cases with one force (P) and two forces (F) are considered.

Optimal topologies and the converged eigenvalue λ_1 for these structures are summarized in Fig. 12. In Fig. 12a, c and e, the structure dimensions are 400×100×4 mm^3 and those of Fig. 12b, d and f are 600×100×4 mm^3. Figure 12a and b are the optimal topologies for considering the out-of-plane buckling of the plate structures, and the optimal designs for considering in-plane buckling of the same structures are illustrated in Fig. 12c-f. In Fig. 12c and e, two concentrated forces (F) are applied and one force P is applied for the structure in Fig. 12d and f as shown in Fig. 1b. The applied resultant force for Fig. 12a-f are 2, 0.8, 60, 30, 60 and 30 (kN), respectively. As λ_{min}=0.001 is used as the constraint, the applied loads are chosen so that $0.1<\lambda_1<10$ in the present computations.

Figure 12a and b are the optimal topologies of the plate buckling, where α=0.5 are used for both plates. It is observed that the obtained optimal topologies are similar to those of the plate (400×200×4 mm^3; α<0.3) in Fig. 8. It is interesting that the critical buckling load of a plate with 75 % material is almost the same as that the full solid plate.

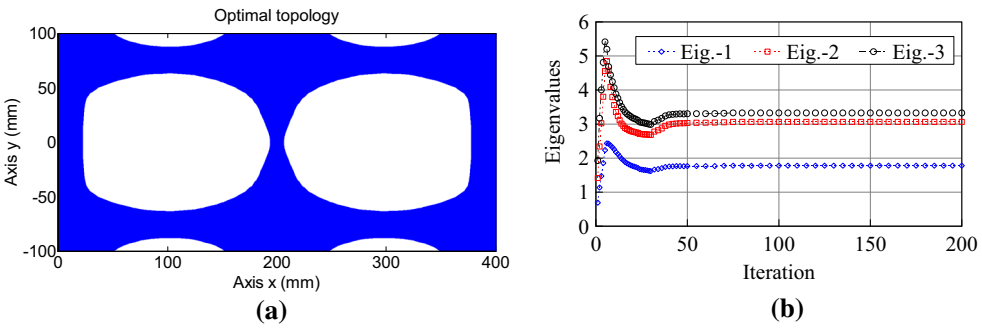

Fig. 10 Optimal topology and eigenvalues of the plate with the enforced displacement when α=0.4 and V_f=0.5 (**a**) optimal topology; (**b**) eigenvalue versus iteration

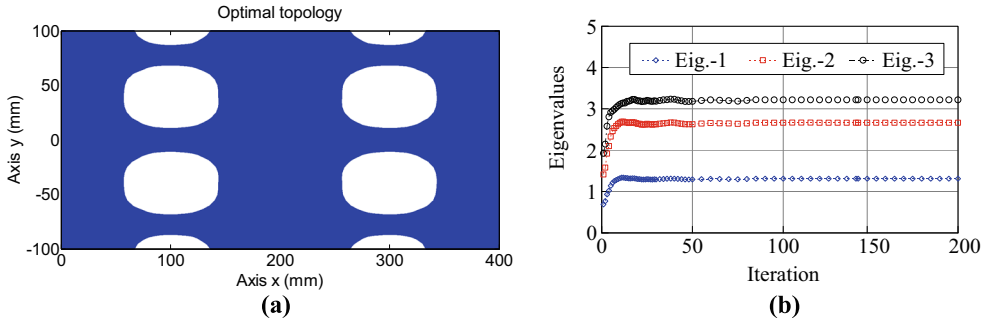

Fig. 11 Optimal topology and eigenvalues of the plate with the enforced displacement when α= 0.15 and V_f=0.75 (**a**) optimal topology; (**b**) eigenvalue versus iteration

Figure 12c-f are for the in-plane buckling of the same structures behaving like a column-beam, where the connectivity coefficient α is not used for Fig. 12c and d and small α values are chosen for Fig. 12e and f. It is seen that, in the optimization involving in-plane buckling of the column-beam, use of the connectivity coefficient may not be necessary as its influence on the buckling load appears to be negligible for the examples considered. However, the connectivity coefficient used for in-plane buckling of the column-beam apparently yields different optimal topologies with enhanced load-path. It is also noted in these numerical examples that the connectivity coefficient may improve convergence rate as the occurrence of mode switching appears to be reduced.

In buckling optimization and other eigenvalue problems for plate structures, user defined reinforcements are often used as non-design domains to create acceptable load-paths (Bendsoe and Sigmund 2003; Niu et al. 2009). It is evident that the present proposed connectivity coefficient can also be effective to serve the purpose of ensuring load-path continuity.

By comparing with the optimal designs in (Bendsoe and Sigmund 2003), the optimal topology in Fig. 12c and d correlate with those obtained by SIMP without reinforcement, and Fig. 12e agrees with that using the reinforcement (Bendsoe and Sigmund 2003). This further confirms the effect of the connectivity coefficient. To the best knowledge of the authors, similar optimal designs for buckling plates obtained in this paper have not been found in open literatures.

It should be pointed out that the assumptions are used in linear buckling analysis, such as 1) small deflection and 2) linear-elastic material; therefore, the applicability is limited to the structures satisfying these conditions.

4.5 Spurious local buckling, mode switch

In the present algorithm, the constraint of ($0<\lambda_{min}<\lambda$) is introduced and used (λ_{min}=0.001) for the present examples. To illustrate the effects of removing this constraint, Table 1 lists the computed eigenvalues λ_1 -λ_6 at iterations 118–121 for the column-beam (600×100×4; α=0; V_f=0.5, see Fig. 12d) subjected to force P. Evidently, λ_1 -λ_4 in these iterations are negative and their associated modes are spurious local eigen modes, and the iterative process will become divergent. However, these spurious local buckling modes can be effectively excluded by the introduced constraint (in all the present computations, λ_{min}=0.001 is used) to achieve a well-behaved convergence.

As λ_{min} (=10^{-3}) is chosen in the present computation, λ_5 and λ_6 of Table 1 are output as λ_1 and λ_2. Figure 13a-c illustrated the Φ function and iso-value surfaces at iterations 118, 119 and 121, and the curve of the eigenvalue versus iteration is plotted in Fig. 13d. By conducting finite element analysis using the input material data $\{\mathbf{x_e}\}$ obtained in iterations 118–121 and examining the 1st and 2nd mode shapes, it is found that the 2nd mode shape at iteration 119 is almost the same as the 1st mode shape at iterations 118, 120 and 121.

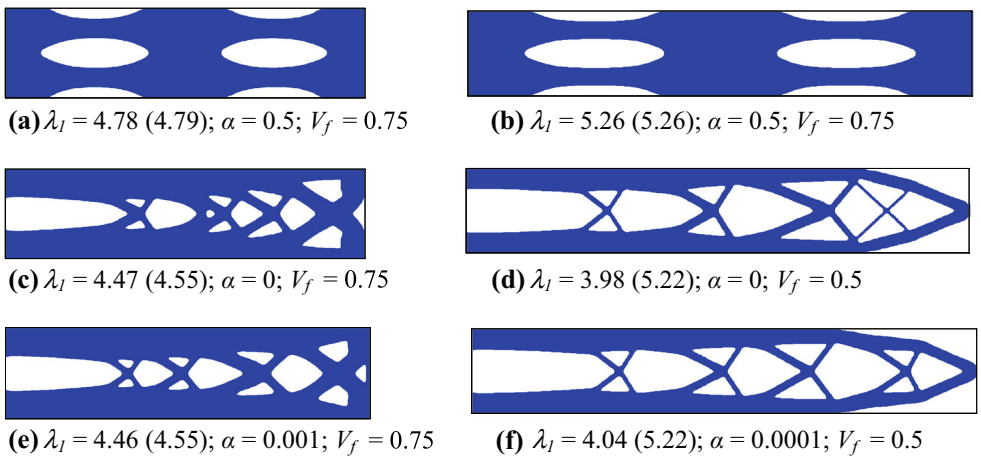

Fig. 12 Optimal topologies and converged eigenvalues of a relatively-narrow plate and column-beam (values in brackets are eigenvalues of corresponding full solid structures)

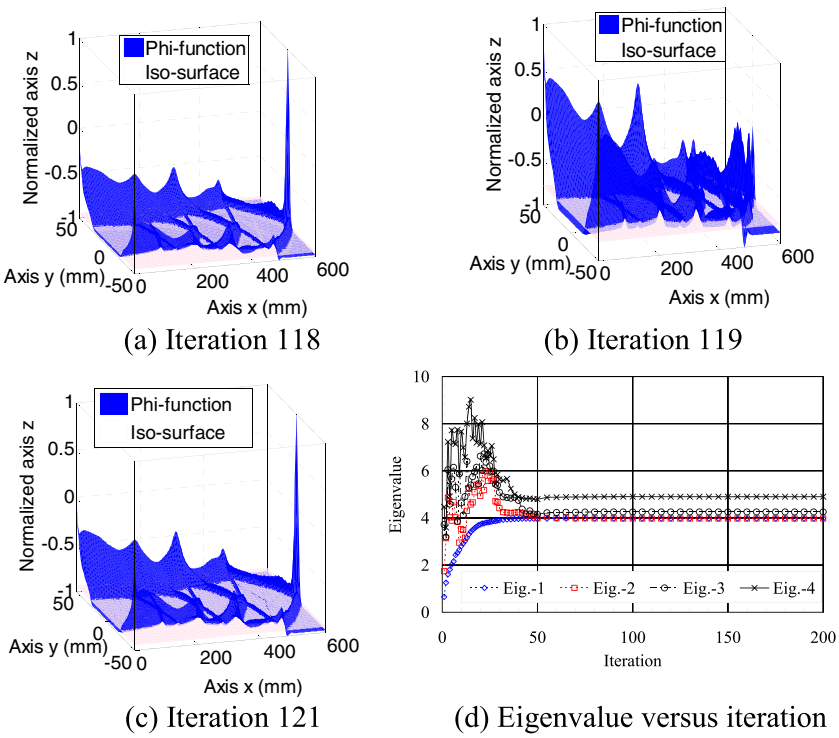

Fig. 13 The Φ function and iso-value surfaces at iterations 118, 119 and 121, eigenvalue versus iteration for the column-beam ($600\times100\times4$; $\alpha=0$; $V_f=0.5$) subjected to force P

Therefore, the 2nd mode shape at iteration 119 could be output in the FEA as the 1st mode shape, namely, the first two modes are switched for the calculation of the Φ function.

Similar to the case for the in-plane buckling of column-beam optimization, we now consider the optimization involving out-of-plane buckling of the plate ($400\times200\times4$; $\alpha=0.10$; $V_f=0.75$; mesh: 120×60; see Fig. 5d) subjected to the distributed load. For this case, Fig. 14 illustrates the Φ function and iso-value surfaces at iterations 32–35. It is apparent that the Φ functions for iterations 32, 34 and 35 resemble each other, whereas that for iteration 33 is completely different. By considering the buckling shapes of a plate with full solid material, it is easy to identify that the Φ function shown in Fig. 14b is related to the 2nd buckling mode. This means that at iteration 33 the 2nd mode shape is output from the FEA rather than the 1st one due to mode switch.

By referring to the weighting factor update approach defined in (7a)-(7c), random occurrence of mode switch can slow down convergence as the weighting factors $\Delta\{\mathbf{x_e}\}_k^{(1)}$ are incorrectly calculated at the k^{th} step. Additional iterations are thereafter needed to remove the effect of the incorrectly assessed variations in weighting factors. Frequent occurrence of mode switch can lead to divergence.

Figures 13 and 14 also indicate that mode switch may be identified possibly by comparing mode shapes for repetitive eigenvalues. However, in the present study, mode switch was identified but no treatment was implemented due to occasional occurrence of mode switches in all examples considered. For example, by ignoring the negative eigenvalues and relabeling the positive ones in Table 1, it is noted that: when $(\lambda_2 - \lambda_1)/\lambda_1 \le 7.54\times10^{-7}$, mode switch may occur (see iteration 119); when $(\lambda_2 - \lambda_1)/\lambda_1 \ge 1.76\times10^{-6}$, mode switch may not take place (see iteration 118, 120 and 121). As NASTRAN has up to 8 effective digits, only eigenvalues with identical first seven effective digits are considered repetitive. For the meshing schemes and material updating model used, repetitive eigenvalues or mode switches occur only occasionally, and they hardly affect iterative convergence (see Fig. 13d as an example).

In the present computations, two methods have been used to track mode switch: 1) record the Φ function and iso-level surfaces as shown in Fig. 13a-c, and 2) calculate $\Delta t^k=|t^k-t^{k-1}|$ and $\Delta\lambda_1^k=|\lambda_1^k-\lambda_1^{k-1}|/\lambda^k$. Method 1) can be used to identify the mode switch after iterative processes. Method 2) can be used in iterations: after iteration N_λ, if $\Delta t^k>\varepsilon_t$ and $\Delta\lambda^k>\varepsilon_\lambda$, the data of mode 2 are extracted and used to construct the Φ function, where ε_t and ε_λ are the tolerances. This method has been tested in the present computation but is not efficient. The difficulties are determination of N_λ, ε_t and ε_λ; this method may also be invalid for the multi-modal problems. It is noted that influences of mode switch in the present algorithm depends on increment $(\{\mathbf{x}_e\}_k^{(3)}-\{\mathbf{x}_e\}_{k-1})$; when it is small, the mode switch slows down the convergent rate only.

5 Effects of soft material

It should be pointed out that the obtained optimal designs contain both solid materials and soft materials (void elements)

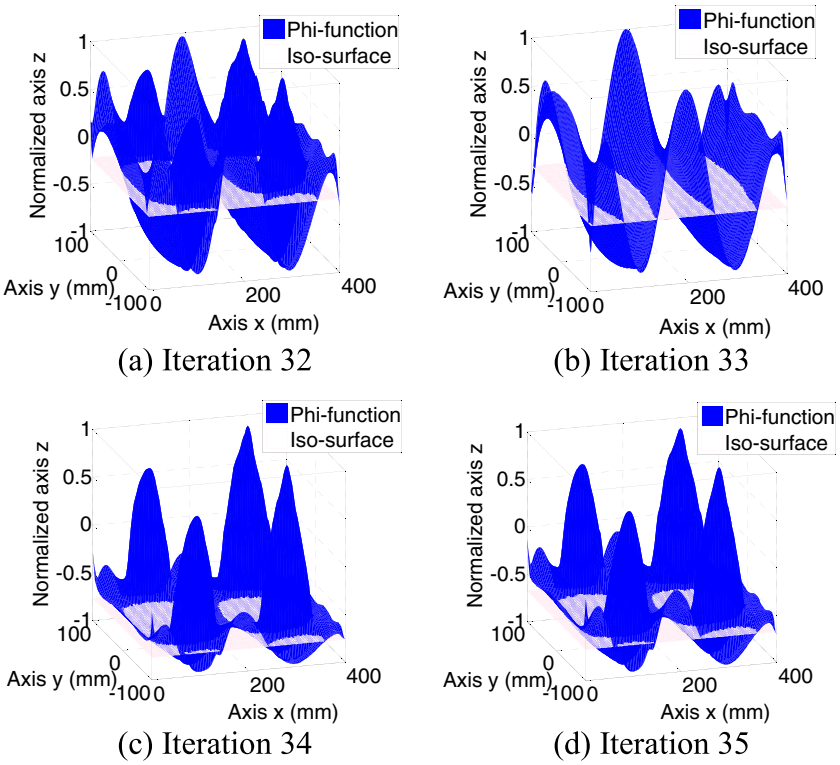

Fig. 14 The Φ function and iso-value surfaces at iterations 32–35 for the plate (400×200×4; α=0.10; V_f=0.75; mesh: 120×60) subjected to uniformly-distributed force

with very small Young's modulus ($10^{-9}E$). It is well known that the effects of these soft materials can be ignored for static analysis cases. However, influences of soft materials on eigenvalue problems, in particular involving buckling, are not well documented.

To study the effects of soft material on buckling related optimum results, let us consider the FEA for five cases: (1) optimal topology with only solid material and clear boundary formed using additional triangular elements as shown in Fig. 15a, (2) completely re-meshed topology with only solid material by modelling boundary using spline functions (see Fig. 15b); (3) the topology with solid and grey materials but with no void material ($x^3_{\min}=10^{-9}$) or elements deleted (see Fig. 15c), (4) the optimal topology with solid, grey and soft material as used in iterations (same as Section 4), and (5) the structure with solid material for entire design domain. In all these FEA computations, $\lambda_{\min}$ was not specified and spurious local mode was not observed as shown in Tables 2 and 3, which list the first five eigenvalues for the plate and column-beam examples for the five FEA cases.

Table 2 lists the eigenvalues for the plate (400×100×4; α=0.5; V_f=0.75) for the five FEA cases. The eigenvalues of cases (1)-(2) are the same and slightly less than those of case (3) (3.13 % for λ_1), which indicates that the topology with clear boundary may be a better choice as it is easy to be fabricated. However, the critical loads for these cases are around 13–15 % lower than those for cases (4) and (5). That is, the inclusion of the soft material can significantly increase the plate buckling load as given in case (4).

Table 3 gives eigenvalues of a column-beam (400×100×4; α=0.001; V_f=0.75) for the five FEA cases. Evidently, buckling factors computed for the five cases are almost the same. This result shows that the inclusion and removal of the soft material part hardly affect the buckling load of a column-beam structure and the critical load using 75 % material volume is about 98 % of that for the full solid structure over the entire design domain.

It is evident that the effects of soft material on buckling optimization are complicated, particularly for plate structures. In optimization for plate structures, thickness may be used as a design variable (Cheng and Olhoff 1981; Bendsoe and Sigmund 2003) or use stiffening ribs with the base thickness (Zhou 2004) to reduce effects of soft material. Alternatively, plate structures with soft material may also be considered in practical structural design and manufacturing.

One of the challenges in optimization for linear buckling structures is considerable effects of soft materials on eigenvalues (Neves et al. 1995; Zhou 2004), particularly for plate structures based on our numerical results. It is known that the 0–1 material model does not accurately depict optimization for plate structures due to the cubic dependence of stiffness on plate thickness (Bendsoe and Sigmund 2003). In linear buckling analysis, the geometric stiffness matrix is computed on

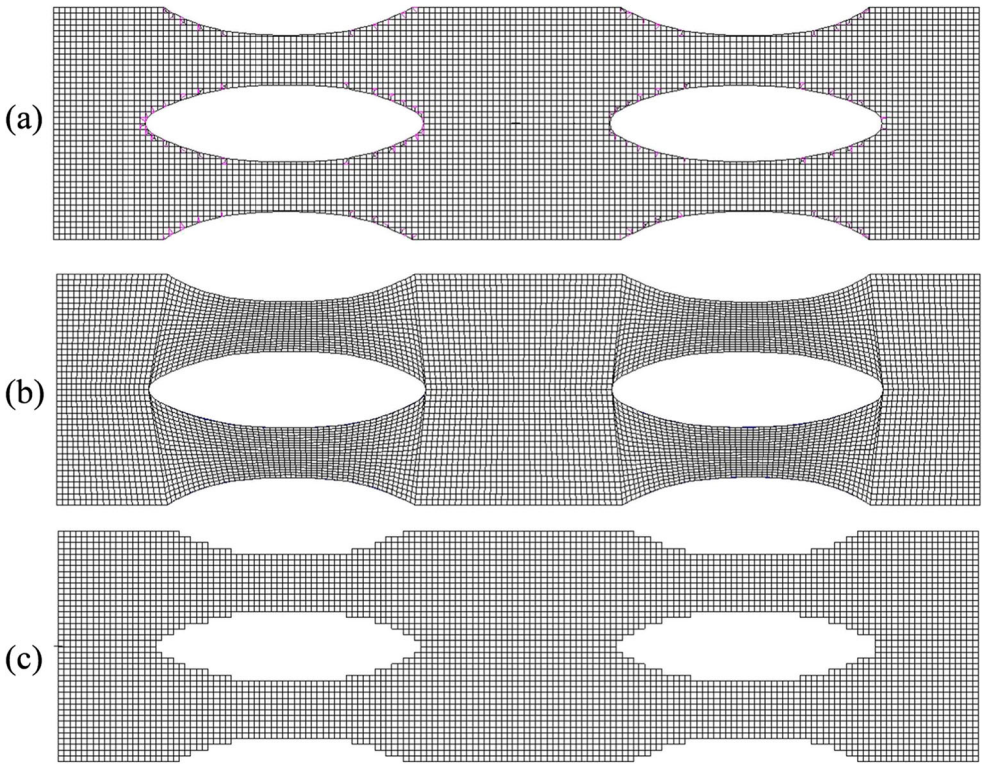

Fig. 15 Finite element meshes for Cases (1), (2) and (3)

the basis of stress distributions obtained in the static analysis for an in-plane problem. It is believed that inaccurate stress distributions and poor description of stiffness in plate elements with low density materials using the 0–1 material model overestimate the buckling load factor.

6 Conclusions

Novel formulation of buckling optimization is defined in (4a) and (4b) where a connectivity coefficient is introduced to ensure the effective load-path and the lower bound of eigenvalue is used to eliminate the spurious modes. MIST is used to study structural topology optimization considering linear buckling, which is demonstrated to be effective and practical. Based on the present numerical results, the following salient points can be drawn: (a) the selected response functions in terms of the strain energy densities of both static stress and eigenvalue analyses are simple and effective; (b) the proposed method of introducing an connectivity coefficient is practical and ensures appropriate load-path continuity; (c) MIST method avoids direct sensitivity analysis and thus the error source of omitting static stress state in sensitivity analysis; (d) void materials or elements have a considerable effect on the out-of-plane buckling loads and a marginal effect on the in-plane buckling loads; (e) the spurious localized mode can be eradicated by specifying the minimum eigenvalue constraint in the present computation.

Table 2 Eigenvalues of a plate (400×100×4; α=0.5; V_f=0.75) with and without soft material

Eigenvalue order	Case (1)	Case (2)	Case (3)	Case (4)	Case (5)
λ_1	4.04	4.04	4.17	4.78	4.79
λ_2	6.38	6.38	6.80	9.81	9.80
λ_3	13.0	13.0	13.8	19.3	19.3
λ_4	17.3	17.3	19.3	29.3	29.3
λ_5	18.3	18.3	20.5	39.4	38.8
λ_1/λ_{10} (%)	84.5	84.5	87.2	99.8	100

λ_{10}: 1st order eigenvalue of the plate with full solid material

Table 3 Eigenvalues of a column-beam (400×100×4; α=0.001; V_f=0.75) with and without soft material

Eigenvalue order	Case (1)	Case (2)	Case (3)	Case (4)	Case (5)
λ_1	4.47	4.51	4.46	4.46	4.55
λ_2	4.70	4.76	4.70	4.70	4.73
λ_3	5.51	5.53	5.44	5.44	5.99
λ_4	11.3	11.2	11.3	11.3	11.4
λ_5	11.4	11.3	11.4	11.4	11.5
λ_1/λ_{10} (%)	98.3	99.2	97.9	97.9	100

λ_{10}: 1st order eigenvalue of the column-beam with full solid material

Acknowledgments The authors are grateful for the support of the Australian Research Council via Discovery-Project Grants (DP110104123 and DP140104408).

Appendix A. Calculation of strain energy density and construction of the Φ function

In MIST, the Φ function is constructed by its nodal values, which can be extracted from elemental data. The strain energy density in static stress analysis and that in buckling analysis for mode 1 in the e^{th} element can be calculated by:

$$E_{sd} = \frac{1}{2}\{\sigma_s^e\}^T\{\varepsilon_s^e\} = \frac{1}{2}\{\mathbf{u_s^e}\}^T[\mathbf{B}]^T[\mathbf{D}][\mathbf{B}]\{\mathbf{u_s^e}\} \quad \text{(A1)}$$

$$E_{\lambda d} = \frac{1}{2}\left\{\boldsymbol{\sigma}_{\lambda_1}^{\mathbf{e}}\right\}^T\left\{\boldsymbol{\varepsilon}_{\lambda_1}^{\mathbf{e}}\right\} = \frac{1}{2k_{\sigma 1}}\{\mathbf{Y_1^e}\}^T[\mathbf{B}]^T[\mathbf{D}][\mathbf{B}]\{\mathbf{Y_1^e}\} \quad \text{(A2)}$$

where $\{\boldsymbol{\sigma}_{\mathbf{s}}^{\mathbf{e}}\}$ and $\{\boldsymbol{\varepsilon}_{\mathbf{s}}^{\mathbf{e}}\}$ are the stress and strain in the static analysis; $\left\{\boldsymbol{\sigma}_{\lambda_1}^{\mathbf{e}}\right\}$ and $\left\{\boldsymbol{\varepsilon}_{\lambda_1}^{\mathbf{e}}\right\}$ are those in buckling analysis for the 1st order mode; [**B**] and [**D**] are the strain–displacement and elastic constant matrices. The strain energy densities at Gaussian points can be determined for element by element by using (A1) and (A2), and then the Φ function surface can be constructed by evaluating their nodal values through averaging the values at the surrounding Gaussian points as in (Tong and Lin 2011; Vasista and Tong 2012) or using other stress or strain recovery techniques.

As an alternative approach, the element-based average strain energy densities for the e^{th} element at static and buckling analyses can be calculated by:

$$E_{sd}^e = \frac{1}{2V_e}\{u_s^{\mathbf{e}}\}^T[\mathbf{k_e}]\{u_s^{\mathbf{e}}\} \qquad (e = 1, 2, \ldots, N_e) \quad \text{(A3)}$$

$$E_{\lambda}^e = \frac{1}{2k_{\sigma 1}V_e}\{\mathbf{Y}_i^e\}^T[\mathbf{k_e}]\{\mathbf{Y_i^e}\} \qquad (e = 1, 2, \ldots, N_e) \quad \text{(A4)}$$

where $[\mathbf{k_e}]$ is the stiffness matrix of the e^{th} element. The nodal values of strain energy densities can be found by using 2nd order polynomial interpolation over adjacent three elements. This alternative approach may be handy as some commercial FEA software can output data of strain energy densities at element centres or even at element nodes. Therefore, the Φ function surface is formed by connecting its nodal values and it will be further normalized to a range [−1, 1] to avoid dealing with too small or large numerals in the present computations.

Appendix B. Interfaces of MIST with MSC NASTRAN

B.1 Create FEA input file

Data input file 'eigen.bdf for NASTRAN is created in the 1st iteration and then modified by using updated element weight factors in the subsequent iterations. In the created/modified input file, the following statements should be included in Sections 'Global Case Control' and 'Bulk Data':

```
Global Case Control:
Subcase 1
TITLE=static analysis
ESE(THRESH=1.E-32)=ALL
Subcase 2
TITLE=buckling analysis
ESE(THRESH=1.E-96)=ALL
Bulk Data:
EIGRL,1, 1.E-3,,10, 0,,,MAX
```

ESE statement used to directly extract elemental strain energies and their densities at each element centre. Very small threshold values are set so that the energy densities at all elements can be output. In the bulk data entry EIGRL, 1.0E-3 or the reasonable positive value must be entered in the 3rd column for satisfying the constraint of $0<\lambda_{\min}<\lambda_1$ to eliminate the spurious local buckling mode.

B.2 Read strain energy densities from the FEA output file

The following function can be used to read the strain energy density at element center in static analysis the 1st order mode from NASTRAN output file 'eigen.f06'.

```
fid=fopen('eigen.f06','r');
Block=1;
while (~feof(fid))
InputTextS=textscan(fid,'%s',1,'delim-
iter','\n');
SS=cell2mat(InputTextS{1,1});
SS1='SUBCASE 1 * TOTAL ENERGY OF ALL
ELEMENTS IN SET';
SS2='EIGENVALUEANALYSISSUMMARY
(READ ODULE)';
TFS1=strncmp(SS,SS1,30);
TFS2=strncmp(SS,SS2,30);
if TFS1
InputTextS=textscan(fid,'%s',2,'delim-
iter','\n');
HeaderLines{Block,1}=InputTextS{1};
NumCols=4;
FormatString=repmat('%f',1,NumCols);
InputTextS=textscan(fid,FormatString,
46);
Data{Block,:}=cell2mat(InputTextS);
[NumRows,NumCols]=size(Data{Block});
```

```
  Block=Block+1;
  elseif TFS2
  break;
  end
  end
  ESES0=cell2mat(Data);
  ESES0(:,1:3)=[];
  ESES(1:Ne, :)=ESES0(1:Ne);
  fclose(fid);
```

The following function can be used to read the strain energy density at element center in buckling analysis for the 1st order mode from NASTRAN output file 'eigen.f06'.

```
  fid=fopen('eigen.f06','r');
  Block=1;
  while (~feof(fid))
  InputText=textscan(fid,'%s',1,'delim-
iter','\n');
  S=cell2mat(InputText{1,1});
  S1='MODE 1 * TOTAL ENERGY OF ALL ELEMENTS IN
SET';
  S2='MODE 2 * TOTAL ENERGY OF ALL ELEMENTS IN
SET';
  TF1=strncmp(S,S1,30);
  TF2=strncmp(S,S2,30);
  if TF1
  InputText=textscan(fid,'%s',2,'delim-
iter','\n');
  HeaderLines{Block,1}=InputText{1};
  NumCols=4;
  FormatString=repmat('%f',1,NumCols);
  InputText=textscan(fid,FormatString,
45);
  Data{Block,:}=cell2mat(InputText);
  [NumRows,NumCols]=size(Data{Block});
  Block=Block+1;
  elseif TF2
  break;
  end
  end
  ESEG=cell2mat(Data);
  ESEG(:,1:3)=[];
  fclose(fid);
```

References

Bendsoe MP, Kikuchi N (1988) Generating optimal topologies in structural design using a homogenization method. Comput Methods Appl Mech Eng 71(2):197–224

Bendsoe MP, Sigmund O (2003) Topology Optimization: Theory, Methods and Applications. Springer, Berlin

Bendsøe MP, Triantafyllidis N (1990) Scale effects in the optimal design of a microstructured medium against buckling. Int J Solids Struct 26(7):725–741

Ben-Tal A, Jarre F, Kočvara M, Nemirovski A, Zowe J (2000) Optimal design of trusses under a nonconvex global buckling constraint. Optim Eng 1(2):189–213

Browne PA, Budd C, Gould NIM, Kim HA, Scott JA (2012) A fast method for binary programming using first-order derivatives, with application to topology optimization with buckling constraints. Int J Numer Methods Eng 92(12):1026–1043

Bruyneel M, Colson B, Remouchamps A (2008) Discussion on some convergence problems in buckling optimisation. Struct Multidiscip Optim 35(2):181–186

Cheng K-T, Olhoff N (1981) An investigation concerning optimal design of solid elastic plates. Int J Solids Struct 17(3):305–323

Cook RD, Malkus DS, Plesha ME (2001) Concepts and applications of finite element analysis, 4th edn. Wiley, New York, c2001

Du J, Olhoff N (2007) Topological design of freely vibrating continuum structures for maximum values of simple and multiple eigenfrequencies and frequency gaps. Struct Multidiscip Optim 34(2):91–110

Eldred MS, Venkayya VB, Anderson WJ (1995) Mode tracking issues in structural optimization. AIAA J 33(10):1926–1933

Kasaiezadeh, A., Khajepour, A. and Jahed, H. (2010). *Using level set method in order to design structures against buckling*. Proceedings of the ASME Design Engineering Technical Conference

Lindgaard E, Dahl J (2013) On compliance and buckling objective functions in topology optimization of snap-through problems. Struct Multidiscip Optim 47(3):409–421

Lund E (2009) Buckling topology optimization of laminated multi-material composite shell structures. Compos Struct 91(2):158–167

Ma Z-D, Kikuchi N, Cheng H-C (1995) Topological design for vibrating structures. Comput Methods Appl Mech Eng 121(1–4):259–280

Manickarajah D, Xie YM, Steven GP (1998) An evolutionary method for optimization of plate buckling resistance. Finite Elem Anal Des 29(3–4):205–230

Manickarajah D, Xie YM, Steven GP (2000) Optimisation of columns and frames against buckling. Comput Struct 75(1):45–54

Mateus HC, Soares CMM, Soares CAM (1997) Buckling sensitivity analysis and optimal design of thin laminated structures. Comput Struct 64(1–4):461–472

MSC.Software (2011). *MD Nastran 2011 & MSC Nastran 2011 Dynamic Analysis User's Guide*. Santa Ana, CA 92707, USA., MSC.Software Corporation

Neves MM, Rodrigues H, Guedes JM (1995) Generalized topology design of structures with a buckling load criterion. Struct Optim 10(2):71–78

Neves MM, Sigmund O, Bendsøe MP (2002) Topology optimization of periodic microstructures with a penalization of highly localized buckling modes. Int J Numer Methods Eng 54(6):809–834

Niu B, Yan J, Cheng G (2009) Optimum structure with homogeneous optimum cellular material for maximum fundamental frequency. Struct Multidiscip Optim 39(2):115–132

Pedersen NL (2000) Maximization of eigenvalues using topology optimization. Struct Multidiscip Optim 20(1):2–11

Pedersen NL, Nielsen AK (2003) Optimization of practical trusses with constraints on eigenfrequencies, displacements, stresses, and buckling. Struct Multidiscip Optim 25(5–6):436–445

Querin OM, Steven GP, Xie YM (1998) Evolutionary structural optimisation (ESO) using a bidirectional algorithm. Eng Comput (Swansea, Wales) 15(8):1031–1048

Rahmatalla S, Swan CC (2003) Continuum topology optimization of buckling-sensitive structures. AIAA J 41(6):1180–1189

Rong JH, Xie YM, Yang XY (2001) An improved method for evolutionary structural optimisation against buckling. Comput Struct 79(3): 253–263

Rozvany GIN (2009) A critical review of established methods of structural topology optimization. Struct Multidiscip Optim 37(3):217–237

Rozvany GIN, Zhou M, Birker T (1992) Generalized shape optimization without homogenization. Struct Optim 4(3–4):250–252

Sekimoto T, Noguchi H (2001) Homologous topology optimization in large displacement and buckling problems. JSME Int J A Solid Mech Mater Eng 44(4):616–622

Sethian JA, Wiegmann A (2000) Structural boundary design via level Set and immersed interface methods. J Comput Phys 163(2):489–528

Sigmund O, Petersson J (1998) Numerical instabilities in topology optimization: a survey on procedures dealing with checkerboards, mesh-dependencies and local minima. Struct Optim 16(1):68–75

Tenek HL, Hagiwara I (1994) "Eigenfrequency maximization of plates by optimization of topology using homogenization and mathematical programming". JSME Int J C Dyn Control Robot Des Manuf 37(4):667–677

Tong LY, Lin JZ (2011) Structural topology optimization with implicit design variable-optimality and algorithm. Finite Elem Anal Des 47(8):922–932

Vasista S, Tong LY (2012) Design and testing of pressurized cellular planar morphing structures. AIAA J 50(6):1328–1338

Wang MY, Wang XM, Guo DM (2003) A level set method for structural topology optimization. Comput Methods Appl Mech Eng 192(1–2):227–246

Xie YM, Steven GP (1993) A simple evolutionary procedure for structural optimization. Comput Struct 49(5):885–896

Yamada T, Izui K, Nishiwaki S, Takezawa A (2010) A topology optimization method based on the level set method incorporating a fictitious interface energy. Comput Methods Appl Mech Eng 199(45–48):2876–2891

Zhao Q, Ding Y, Jin H (2011) A layout optimization method of composite wing structures based on carrying efficiency criterion. Chin J Aeronaut 24(4):425–433

Zhou M (2004) Topology optimization for shell structures with linear buckling responses. Computational Mechanics, WCCM VI, Beijing

Zhou M, Rozvany GIN (1991) The COC algorithm, part II: topological, geometrical and generalized shape optimization. Comput Methods Appl Mech Eng 89(1–3):309–336